Performance of the far-IR beamline of the 6 MeV tabletop synchrotron light source

Md. Monirul Haque,[a] Hironari Yamada,[a,b,c]* Ahsa Moon[b] and Mami Yamada[c]

[a]Faculty of Science and Engineering, Ritsumeikan University, 1-1-1 Noji-higashi, Kusatsu, Shiga 525-8577, Japan, [b]Synchrotron Light Life Science Center, Ritsumeikan University, 1-1-1 Noji-higashi, Kusatsu, Shiga 525-8577, Japan, and [c]Photon Production Laboratory Ltd, Ritsumeikan University, 1-1-1 Noji-higashi, Kusatsu, Shiga 525-8577, Japan. E-mail: hironari@se.ritsumei.ac.jp

The performance of the far-infrared (FIR) beamline of the 6 MeV tabletop synchrotron light source MIRRORCLE-6FIR dedicated to far-infrared spectroscopy is presented. MIRRORCLE-6FIR is equipped with a perfectly circular optical system (PhSR) placed around the 1 m-long circumference electron orbit. To illustrate the facility of this light source, the FIR output as well as its spectra were measured. The optimum optical system was designed by using the ray-tracing simulation code *ZEMAX*. The measured FIR intensity with the PhSR in place is about five times higher than that without the PhSR, which is in good agreement with the simulation results. The MIRRORCLE-6FIR spectral flux is compared with a standard thermal source and is found to be 1000 times greater than that from a typical thermal source at ~ 15 cm^{-1}. It is also observed that the MIRRORCLE-6FIR radiation has a highly coherent nature. The broadband infrared allows the facility to reach the spectral range from 10 cm^{-1} to 100 cm^{-1}. MIRRORCLE-6FIR, owing to a large beam current, the PhSR mirror system, a large dynamic aperture and small ring energy, can deliver a bright flux of photons in the FIR/THz region useful for broadband spectroscopy.

Keywords: high-current tabletop synchrotron; photon storage ring; 6 MeV MIRRORCLE; Fourier-transform infrared spectroscopy; broadband spectrum.

1. Introduction

Fourier-transform infrared spectroscopy (FTIRS) is now among the main analytical tools in materials and life science. It has many well known advantages including simplicity of use. In the far-infrared (FIR) and terahertz (THz) region, however, the use of FTIRS has been greatly limited because of the lack of brilliant and high-flux light sources. The THz and sub-THz region spectra are of great importance owing to the rich chemical and physical processes occurring in these ranges (Ferguson & Zhang, 2002; Fitch *et al.*, 1970; Chantry, 1971). In particular, the FIR plays a great role in the analysis of water, proteins, biological tissues, cancers and chemical reactions, since they have broadband spectral range. However, there is still a lack of powerful FIR sources in the world.

In recent years it has become apparent that synchrotron radiation is a useful source for IR spectroscopy. The first advantage of synchrotron radiation (SR) is its large spectral extension: it can produce high flux from the X-ray to infrared region, and in particular in the far-infrared and submillimetre ranges. Different from a conventional thermal source, the synchrotron infrared source has a pulsed structure with typically some 100 MHz duration. These pulses are a direct consequence of the manner in which a synchrotron operates.

Numerous beamlines that are dedicated to infrared spectroscopy have been developed at SR facilities all over the world. It is noteworthy that as the field is gaining maturity IR beamlines are becoming more specialized and now cover the fields of surface science (Lobo *et al.*, 1999; Surman *et al.*, 1999), high-pressure studies (Schade *et al.*, 2002; Kimura *et al.*, 2006), spectromicroscopy (Martin & McKinney, 2001; Kimura *et al.*, 2001), high-resolution molecular studies (Hegelund *et al.*, 2003) and condensed-matter far-infrared spectroscopy (Dumas *et al.*, 2006; Byrd *et al.*, 2004) *etc.* In the case of the synchrotron infrared from a bending magnet, an ideal storage ring would be one equipped with a large bending radius (for low emittance), large stored current, large aperture (for high flux) and low ring energy (for low heat load). In general, third-generation rings for X-rays have a low emittance of the IR beam.

The MIRRORCLE-type synchrotron light sources are unique owing to the following properties: an electron energy lower than 20 MeV, a storage-ring orbit radius as small as 8 cm (for the 1 and 4 MeV types) (Hasegawa & Yamada, 2007) and 15 cm (for the 6 and 20 MeV types) (Yamada, 2003, 2004), a stored ampere-order beam current circulating in a full circular electron orbit of radius 156 mm, and a compact magnet yoke diameter of 35 cm (for the 1 and 4 MeV types), 60 cm (for the

299

research papers

Table 1
Specifications of MIRRORCLE-6FIR.

Electron energy	6 MeV
Storage ring orbit radius	156 mm
Storage ring magnetic field	0.128 T
Maximum stored current	3 A
Injector peak current	100 mA
Injection repetition at maximum	400 Hz
Pulse width	100 ns
Injection method	1/2 resonance

6 MeV type) and 80 cm (for the 20 MeV type). In spite of its low electron energy, the MIRRORCLE-type synchrotron generates milliwatt-order submillimetre-range FIR radiation (Yamada, 1997, 1998; Kleev *et al.*, 1995; Moon *et al.*, 2007). The low ring energy, large dynamic aperture and large stored current are advantageous for obtaining a FIR photon beam with a higher flux; thus it is useful for broadband reflections as well as absorption spectroscopy.

As the MIRRORCLE-type synchrotrons are low-energy storage rings, they cannot compete with large storage rings such as SPring-8 at the higher photon energies. However, they can surpass them in the FIR and THz regions by collecting synchrotron radiation with a wider acceptance angle. So far the useful FIR has been produced by making use of MIRRORCLE-20 (Yamada, 2003) to analyze water, aqueous solutions, proteins *etc.* (Yamada, 1997; Miura *et al.*, 2007). We have learned, however, that the smaller machine MIRRORCLE-6X (Yamada, 2004) produces more FIR owing to its different injection mode mechanism (1/2 resonance). Therefore, we have constructed a new beamline, MIRRORCLE-6FIR, by using the 6 MeV MIRRORCLE storage ring. A perfectly circular optics, known as the photon storage ring (Yamada, 1989), is an important device for this beamline. The photon storage ring collects SR photons from the whole arc of the electron orbit as well as acting as an optical resonator. We have designed such an optical resonator for MIRRORCLE-6FIR and employed it as the first mirror inside the vacuum chamber. The specifications of MIRRORCLE-6FIR are listed in Table 1.

In §2 we describe the entire layout of the beamline; we also present the design of a new circular optics. §3 addresses the ray-tracing simulation made using the computer code *ZEMAX*. In §4 we discuss the experimental results including FIR output, FTIR spectra and beam dynamics in MIRRORCLE-6FIR. The coherent nature of the FIR owing to the photon storage ring mechanism is also discussed.

2. Beamline layout

In contrast to bending-magnet beamlines for vacuum-ultra-violet or X-rays, an infrared beamline requires large extraction optics owing to the increasingly large angles into which synchrotron radiation is emitted as wavelengths increase. This angle is given by (Duncan & Williams, 1983)

$$\theta\,(\text{rad}) = 1.6(\lambda/\rho)^{1/3}, \tag{1}$$
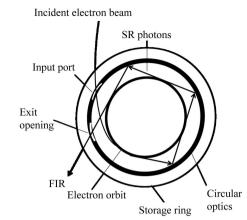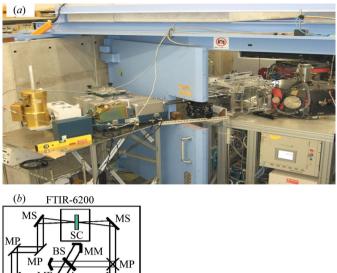

Figure 1
The beamline optics in the MIRRORCLE-6FIR storage ring made of a normal conducting magnet having a bending radius of 156 mm. A perfectly circular optics of radius 217.3 mm has been installed around the electron orbit to accumulate synchrotron radiation, and to generate stimulated emissions.

where ρ is the electron orbit bending radius and λ is the wavelength (in the same units as ρ). Thus, efficient extraction of the infrared from a synchrotron is increasingly difficult towards longer wavelengths. An exit opening on the circular mirror surface, designed for the MIRRORCLE-6FIR beamline, can collect a solid angle of 264 × 198 mrad. The MIRRORCLE-6FIR ring has a bending radius of 156 mm; therefore the beamline collects (per horizontal angle) 100% of the infrared down to 14 cm^{-1}. The beamline can be viewed as having two sections: a high-vacuum (UHV) section directly connected to the ring vacuum, and a low-vacuum section containing the optics for transferring and splitting the beam to the FTIR endstation. The two sections are separated by a 50 mm clear aperture, a 3 mm-thick Tsurupica (Pakkusu, Japan) window. The transmittance of this window is about 85% for $\lambda > 50$ µm (Moon *et al.*, 2007).

The beamline optics in the ring vacuum of MIRRORCLE-6FIR is shown in Fig. 1. It is composed of only one circular concave mirror concentric with the electron orbit of radius 156 mm. The circular optical system can collect SR photons emitted into 2π of the electron orbit, and so it is also known as the photon storage ring (PhSR) (Yamada, 1989, 1991). A key characteristic of the PhSR is the reflection of collected synchrotron radiation to intersect the electron orbit again. This configuration, under certain circumstances, induces lasing and significantly boosts FIR output by an order of magnitude. In this sense the circular mirror surrounding the electron orbit also acts as an optical resonator, playing a role in high intense FIR generation. The mirror fabricated for MIRRORCLE-6FIR is made of aluminium. This material is selected because of its rigidity and good FIR reflectivity. The mirror curvature is made with a 0.1 µm tolerance. For a 100 µm wavelength we selected a mirror width of $D = 38$ mm, with curvature in the axial direction of $R_0 = 125.81$ mm and a mirror radius of $R = 217.3$ mm.

Fig. 2 shows a photograph of the FTIR beamline and a schematic drawing of its optical system. The exit opening of
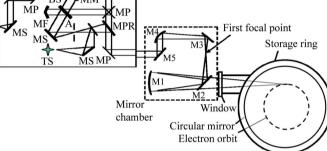
Figure 2
(*a*) Photograph of the FTIR beamline, and (*b*) schematic drawing of the optical system for this beamline. The circular mirror, made of Al, is placed around the electron orbit inside the storage ring. It can collect the SR photons from the whole arc of the electron orbit. MP, MS, MM, MF and MPR represent plane, spherical, moving, fixed and parabolic mirrors. BS is a Mylar beam-splitter. A and SC represent the variable aperture and sample cell. TS is an internal thermal source. A defines the effective source size of the thermal source as well as of the synchrotron source; in this experiment it was 2 mm diameter.

Table 2
Calculated mirror radius for wavelength $\lambda = 100$ μm.

Beam energy $E_e = 6$ MeV, electron orbit radius $\rho = 0.156$ m, harmonics $h = 8$.

λ (μm)	n	θ (rad)	R (m)
100	1	0.924997	0.258271
100	1/2	0.773614	0.217276
100	0	0.116	0.156488

entrance aperture of 12.7 mm at a focal ratio of 3.8, an exit aperture of 1.8 mm, a diamond area of diameter 2.5 mm, and a sensitivity of 2.53×10^5 V W^{-1}.

2.1. Designing the mirror radius

The light pulses confined in the mirror cavity propagate along a single photon path finally leading to the exit opening, and form a pulse train with an exact time period. The Fourier transform of this pulse train corresponds to the frequency of the light wave. The wavelength to be enhanced by the PhSR is actually determined by the mirror radius relative to the electron orbit radius (Yamada, 1997, 1998, 1989). So the design of a suitable mirror radius is of prime importance. The following two formulae are used to calculate the mirror radius,

$$\lambda = 2\left(\theta + \frac{n\pi}{h}\right)\frac{\rho}{\beta} - 2\rho\cos\alpha\tan\theta, \qquad (2)$$

$$R = \frac{\rho\cos\alpha}{\cos\theta}, \qquad (3)$$

where λ is the wavelength of the light pulse, θ is the phase between the light pulse and the electron, α is the phase shift owing to the beam size, ρ is the electron orbit radius, R is the mirror radius (see Fig. 3), n is an integer indicating the nth electron bunch which merges with the light pulse, h is the harmonic number and β is the normalized electron velocity. Equation (2) is solved as a function of θ for different values of n, and then the mirror radius is calculated using equation (3). The calculated values are listed in Table 2.

size 40 × 30 mm on the circular mirror surface allows SR photons to be extracted from the storage ring body, and to move directly to the radiation window. The infrared light is extracted from the ring by a set of two mirrors: M2 is a plane mirror while M1 is a concave mirror that images the source point at the first focal point. The concave mirror and the first focal point are located at 600 mm and 1163 mm, respectively, from the SR emission point. The beam is then deflected by two plane mirrors M3 and M5, and reformed in a parallel beam by parabolic mirror M4, then introduced into a commercial FTIR-6200 instrument. The concave mirror, plane mirrors and parabolic mirror are enclosed in a vacuum chamber as shown in Fig. 2(*b*). The FTIR-6200 (JASCO, Japan) has a Michelson-type interferometer, a step-scanning system for its moving mirror, and a function for time-resolved measurements. The instrument can be used with both the SR source and its internal thermal source. The FTIR-6200 covers the energy range from the far-IR to the near-IR regions of 1 meV to 0.97 eV (10–7800 cm^{-1}) by choosing suitable beam splitters and optical elements. The detector is a Si bolometer (Infrared Lab, USA), model 3118 of composite type, operating at a temperature of 4.2 K. The detector characteristics are an
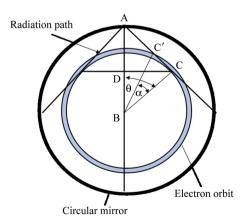

Figure 3
Schematic view of the circular mirror. AB = R is the mirror radius, BC = ρ is the electron orbit radius, and AD = R_0 is the vertical curvature of the mirror. θ is related to the phase between the light pulse and the electron, and α is the phase shifted owing to the finite beam size.

Table 3
Calculated vertical curvatures R_0 corresponding to different orbit radius ρ.

σ_x is the radial beam size and R is the mirror radius.

σ_x (m)	ρ (m)	R (m)	R_0 (m)
±0.015	0.171	0.2173	0.082735
±0.015	0.156	0.2173	0.105307
±0.015	0.141	0.2173	0.125809

According to the resonance condition, it is important to choose a value of n to obtain a suitable mirror radius. The value $n = 0$ represents the case in which the interaction of the radiation occurs always with the same electron bunch. This case is called the 'whispering gallery mode' (Keller & Rubinow, 1960; Weinstein, 1969; Mima *et al.*, 1991). This mode, however, is inadequate for the PhSR because the optical resonator has to be set too close to the electron orbit, and also the power loss owing to the ohmic loss becomes too large (Yamada, 1998). Since we need a space between the optical resonator and the electron orbit, a higher value of n is suitable. Considering this, we have chosen the value of n as 0.5, and the corresponding mirror radius as 217.3 mm. This value of n implies that a photon beam touches the electron orbit at every 0.5 interval as well as a full interval of electron bunches.

2.2. Designing the vertical curvature

The PhSR also functions like an undulator by causing the electron trajectory and the radiation path to cross. The vertical profile of the mirror is designed so as to focus the photon beam onto the electron orbit, and thereby forces SR photons and electrons to be merged at an angle, which is an essential condition for coherent generation. In the calculation of the vertical curvature we have taken three orbits into consideration: the outermost, central and innermost. Since the central orbit radius is 156 mm and the radial beam size is about ±15 mm for MIRRORCLE-6FIR before damping, the radii of the outermost and innermost orbit become 171 mm and 141 mm, respectively. The vertical curvature has been calculated using the following equation (Kleev *et al.*, 1995),

$$R_0 = \frac{R^2 - \rho^2}{R}, \qquad (4)$$

where R is the mirror radius, ρ is the electron orbit radius and R_0 is the vertical curvature (see Fig. 3). Since a long vertical curvature is good for reducing the escape of light pulses, we have chosen the largest curvature, $R_0 = 125.83$ mm, which corresponds to the innermost orbit. The calculated vertical curvatures using the above equation are listed in Table 3 for three different orbit radii.

3. Ray-tracing simulation

The whole optics was simulated using the ray-tracing program *ZEMAX-EE* (Engineering Edition) to determine the optimum optical system. A special type of light source
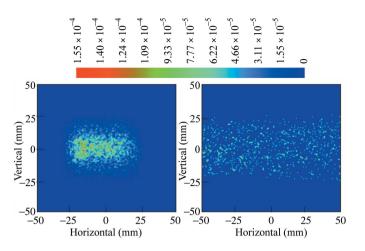

Figure 4
Ray-tracing results at the exit port obtained using the simulation code *ZEMAX*. Characteristics of FIR emission are an emission angle of ±85 mrad at each electron position, and a photon energy of 0.01 eV (~100 μm). The left-hand image is observed with the PhSR circular mirror having an exit opening of size 40 × 30 mm; the right-hand image is without the circular mirror. The calculated photon density with the circular mirror (PhSR) (left) is about eight times larger than that without the PhSR (right).

modelled by DLL (Windows Dynamic Link Library) was used in order to support the desired properties of the MIRRORCLE-type synchrotron. The sources were placed at different angles along an orbit of radius 156 mm. The power of each source was set at 30 μW. The electron beam profile is simulated by a Gaussian curve with $\sigma_h = \pm 10$ mm and $\sigma_v = \pm 1.5$ mm. The emission angle of SR light in both directions is ±85 mrad at a photon energy of 0.01 eV, which is very large compared with that of other FIR dedicated sources (Williams, 2002; Kimura *et al.*, 2006). Toroidal surfaces consisting of a rectangular surface with a possibly aspherical toroidal shape were placed around the source orbit for circular optics. The horizontal and vertical curvatures of this optical system were set to 217.3 mm and 125.81 mm, respectively, as listed in Tables 2 and 3.

Fig. 4 shows the radiation distribution observed at the exit of the storage ring port at a photon energy of 0.01 eV ($\sim$100 cm^{-1}). The radiation intensity was calculated using an imaginary detector for both with and without a circular mirror. The left-hand figure shows the case in which a circular mirror is placed around the electron orbit, while the right-hand figure shows the case without a circular mirror. Note that the photon beam size is different because of the difference in acceptance angle. The size of the imaginary detector, 100 × 100 mm, is the same for both cases, but in the case with a circular mirror placed around the electron orbit the horizontal acceptance is limited by its exit port of size 40 × 30 mm. The calculated photon intensity for the above machine parameters is about eight times higher for the case with the circular mirror than for that without. A high-power FIR emission is expected with this PhSR mirror system and large stored beam current.

4. Results and discussion

4.1. Photon storage ring FIR output

Fig. 5 shows the measured FIR intensity with and without the PhSR as a function of incident beam current. The FIR intensity was measured using a cooled Si bolometer placed directly at the surface position of the exit channel of the storage ring. At 100 mA beam current the FIR intensity measured with the PhSR is about five orders higher than that measured without the PhSR, which is in good agreement with the simulation result found using *ZEMAX* (see Fig. 4). This result indicates that the new circular optics designed for MIRRORCLE-6FIR is working. We expect that the radiation intensity boosted by this optical system can be further increased by increasing its radiation collection efficiency.

An important result observed in this experiment is that the FIR intensity measured with the PhSR is proportional to $I^{1.8}$, where I is the injector beam current, but for the case without the PhSR it is simply linear with I. This linearity must indicate a highly coherent nature of the PhSR FIR radiation. Coherent radiation is known in synchrotrons in which radiation is emitted from electrons in a short bunch all in the same phase, thus giving an I^2 tendency. For our case it gives $I^{1.8}$ and this appears when the circular mirror is associated.

It is known that coherent synchrotron radiation (CSR) is dominant in the range of wavelengths comparable with or longer than the longitudinal bunch length. Under this condition the electrons emit photons in phase and a single-cycle electromagnetic pulse results with intensity proportional to the square of the number of electrons in the bunch (Michel, 1982; Hirschmugl *et al.*, 1991). Our PhSR output, however, is not CSR, which appears only when the PhSR mirror is applied.

Interference effects of synchrotron radiation between successive bunches have been proved experimentally to be important (Wingham, 1987). Including the effect of CSR and the successive bunches, Yamada proposed the formalism for PhSR under the circular mirror (Yamada, 1997, 1998) as
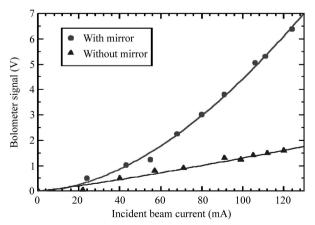

Figure 5
Beam current I dependence of FIR intensity. The dependence is $I^{1.8}$ with the PhSR circular mirror, but simply linear without the circular mirror. FIR output of the PhSR is highly coherent but is not lasing.

$$P(\lambda)\,d\Omega\,d\lambda = p(\lambda)hN_e[1 + (N-1)F(\lambda)]G(\lambda)\,d\Omega\,d\lambda$$
$$\cong p(\lambda)hN_e[1 + N_eF(\lambda)]G(\lambda)\,d\Omega\,d\lambda, \quad (5)$$

where $P(\lambda)$ is the incoherent synchrotron radiation power from one electron, h is the harmonic number, N_e is the number of electrons in the bunch and $F(\lambda)$ is the form factor which is the Fourier transform of the longitudinal electron distribution in the bunch. The function $G(\lambda)$ represents the interference between the coherent rays as well as between the incoherent rays as a result of the reflection owing to the surrounding mirror (PhSR). This is given for a certain reflection coefficient f as

$$G(\lambda) = \left[\sum_r^{N_b}\left(f^{1/2}\right)^r \sin(r\pi\lambda/\lambda_R)/\sin(\pi\lambda/\lambda_R)\right]^2$$
$$\cong \left[\sum_r^{N_b}\left(f^{1/2}\right)^r\right]^2\left[\sin\left(\bar{\bar{N}}\pi\lambda/\lambda_R\right)/\sin(\pi\lambda/\lambda_R)\right]^2, \quad (6)$$

where N_b is the number of bounces owing to the circular mirror, and λ_R is the resonance wavelength. According to the above equations the SR power from the PhSR is proportional to the square of the electron number N_e in the bunch and to the square of the averaged number of interaction times $\bar{\bar{N}}$.

Since the bunch length of MIRRORCLE-6FIR is $\sim$10 mm, however, which is very long compared with the emitted wavelength of radiation, the coherent enhancement owing to the short bunch must be insignificant. However, practically we observe the coherent nature of the PhSR FIR radiation (see Fig. 5), generating a new research ramification. The bunch length in the storage ring in this experiment is determined by the injector RF acceleration system, which is 2.25 GHz. We usually operate the storage ring without the continuous wave acceleration applied. So the time structure of the injector appears, and is eight harmonics, since the orbit circumference of the ring is exactly eight times the injector RF wavelength. The injector bunch size is known to be about 10 mm long.

We can think of two reasons for this partially coherent phenomenon. Firstly, interference effects of stored SR photons and the electron beam should appear. In fact, the PhSR not only collects SR photons but also functions as an undulator with an infinite number of periods. In the PhSR, photons are bounced or wiggled periodically by the circular mirror instead of wiggling electrons, which leads to the modulation of electron density and to lasing. In the present PhSR system the modulation of electron density could be developed although the laser gain is small. The partial modulation of the electron beam might lead to the partial coherence as indicated as 1.8.

Secondly, the effect of space coherence may play an important role. The longitudinal bunch length of MIRRORCLE, which is determined by the injector, is about 10 mm, but the energy distribution of the injector microtron is about 0.2%. As a result the individual bunch radial width is less than 1 mm in both vertical and horizontal directions. So this radial size of less than 1 mm may generate partial space coherence.

4.2. FTIR spectra

Fig. 6 shows the spectra obtained with both the PhSR source and the spectrometer's internal thermal source (a ceramic heater of diameter 7.1 mm at 1500 K). The measured spectra are over the frequency range from 10 to 100 cm^{-1} (1–12 meV). The red curve shows the SR spectrum and the violet curve is for the thermal source. The SR spectrum was recorded at an injection beam current of 120 mA and an aperture size of 2 mm at the focusing point. The position of the aperture is shown as A in Fig. 2(b). This aperture actually defines the size of the emitter point or source point of the internal source as well as the SR source. The relative signal levels of synchrotron radiation compared with the thermal source are also shown in Fig. 6 (green curve). The drop near 72 cm^{-1} for both the SR and thermal spectra is due to absorption by the bolometer filter. The Si bolometer detector, model 3118, of composite type uses a 100 cm^{-1} far-infrared cut-on type filter consisting of 0.75″ diamond wedged crystal quartz, 1 mm thick, coated on one face with garnet powder.

The beamline allows radiation to be collected at lower wavenumbers than 10 cm^{-1} (e.g. λ = 1000 μm) and, more importantly, maintains the pulsed nature of the synchrotron source for use in broadband time-resolved spectroscopy. It is remarkable that the SR spectrum is much broader and more intense than that of the thermal source below 77 cm^{-1}. The MIRRORCLE synchrotron advantage approaches a factor of 41 at 17 cm^{-1}. We note that the spectra were recorded with a 2 mm-size aperture, which indicates that emission from the 2 mm-size spot on the electron beam cross section contributes to this FTIR measurement, but not the whole emission from the whole beam size.

A typical IR spectrometer uses a thermal source with dimensions of a few millimetres. The Michelson-type spectrometer's source is large, and the source collection optics has an effecti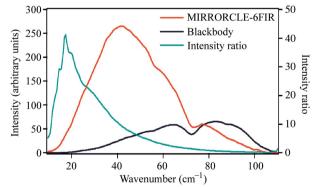ve f number of 3. In spite of such a large and high-temperature thermal source, our SR source outperforms the thermal source. It is quite large compared with that observed by other groups (Lobo et al., 1999). This is due to the advantages of the PhSR and the large beam current.

4.3. Absolute photon flux

We obtain the absolute spectral photon flux of MIRRORCLE-6FIR by using a reference photon source. The reference source is a 1500 K blackbody internal source of FTIR. When the temperature of the blackbody is known, the absolute photon flux is given by the Planck formula,

$$B(\lambda) = \frac{2hc^2}{\lambda^5} \frac{1}{\exp(hc/\lambda KT) - 1}. \tag{7}$$

The observed spectral flux $O_T(\lambda)$ is connected to the Planck formula by the efficiency of the system, $R(\lambda)$, as

$$O_T(\lambda) = R(\lambda)B(\lambda)\, d\lambda\, d\Omega_T\, dA_T, \tag{8}$$

where $d\lambda$, $d\Omega$ and dA are the bandwidth, acceptance solid angle and cross section of the emitter contributing to the measured flux. On the other hand, the measured SR spectrum $O_S(\lambda)$ is connected to the absolute spectral flux $P_S(\lambda)$ as

$$O_S(\lambda) = R(\lambda)P_S(\lambda)\, d\lambda\, d\Omega_S\, dA_S. \tag{9}$$

The efficiency of the system $R(\lambda)$ must be almost the same for the thermal and SR sources. Consequently the absolute spectral photon flux can be obtained by the following formula,

$$P_S(\lambda) = \frac{O_S(\lambda)}{d\lambda\, d\Omega_S\, dA_S} \frac{B(\lambda)\, d\lambda\, d\Omega_T\, dA_T}{O_T(\lambda)}. \tag{10}$$

Here, $d\Omega_T(\lambda)$ and dA_T are defined by the aperture of MS and A in Fig. 2, respectively; $d\Omega_S(\lambda)$ and dA_S are defined by the aperture of M1 and A, respectively. Since the distance between TS and MS is one-fifth shorter than that between the SR source and M1, then $d\Omega_S = d\Omega_T/5^2$. Again, since the focusing distance ratio $(f_1{:}f_2)$ is set to 1:1 for both SR and thermal beamlines, the aperture A gives $dA_S = dA_T = \pi(1)^2 = 3.14$. The ratio $O_S(\lambda)/O_T(\lambda)$ is obtained from the observed spectra in Fig. 6.

Fig. 7 shows the measured (red line) and calculated (green line) spectral photon flux from MIRRORCLE-6FIR, and a blackbody light source (blue line) at a temperature of 1500 K. The measured photon flux of MIRRORCLE-6FIR is almost 1000 times higher than that of the thermal source at lower photon energy (i.e. in the FIR/THz region). The photon flux measured in the present work was also compared with that at other FIR beamlines at different SR sources (see Table 4) and revealed substantial benefits for FIR spectroscopy. Note that the fluxes for other beamlines at four different wavelengths (λ = 10, 100, 500, 1000 μm) were roughly reproduced from their respective references following the same formalism as described above. We observe that the photon flux of MIRRORCLE-6FIR in the THz region is comparable with that of the UVSOR-II and NSLS sources. This is due to the wide acceptance angle and the high beam current of MIRRORCLE-6FIR. We conclude that MIRRORCLE-6FIR

Figure 6
FIR spectra of the PhSR (red line) at 120 mA beam current and 100 Hz injection are compared with that of a ceramic heater (violet line) of diameter 7.1 mm at 1500 K by the FTIR with a cooled Si bolometer. The drop near 72 cm^{-1} is due to absorption in the diamond wedged crystal quartz of the bolometer filter. The green line indicates their intensity ratio indicated on the right. It is seen that the PhSR provides more photons than the thermal source below 77 cm^{-1}. At 17 cm^{-1} the PhSR advantage approaches a factor of 41 with a 2 mm-size aperture, which is indicated as A in Fig. 2(b).

Table 4
Comparison of the photon flux of MIRRORCLE-6FIR with other SR sources.

The flux for the other SR sources has been roughly reproduced from their respective references.

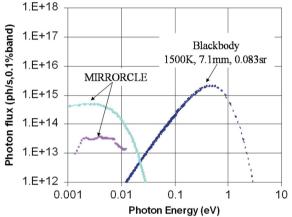|	Photon flux [photons s^{-1} (0.1% bandwidth)$^{-1}$]			
	$\lambda = 10\ \mu m$	$\lambda = 100\ \mu m$	$\lambda = 500\ \mu m$	$\lambda = 1000\ \mu m$
MIRRORCLE-6FIR (calculated)		$\sim 7.85 \times 10^{13}$	$\sim 5.08 \times 10^{14}$	$\sim 4.15 \times 10^{14}$
(measured)		$\sim 1.32 \times 10^{13}$	$\sim 3.06 \times 10^{13}$	$\sim 1.38 \times 10^{12}$
SPring-8 (Kimura *et al.*, 2001)	$\sim 1 \times 10^{13}$	$\sim 3 \times 10^{11}$		
UVSOR-II (Kimura *et al.*, 2006)	$\sim 2 \times 10^{14}$	$\sim 1 \times 10^{14}$	$\sim 2 \times 10^{13}$	$\sim 6 \times 10^{12}$
NSLS (Williams, 2002)	$\sim 10^{12}$	$\sim 10^{13}$	$\sim 10^{14}$	$\sim 10^{14}$
Tohuku-300 MeV linac (Ishi *et al.*, 1991)		$< 10^{10}$	$\sim 1 \times 10^{13}$	$\sim 3 \times 10^{13}$
MLS (Muller *et al.*, 2006)	$\sim 2 \times 10^{14}$	$\sim 8 \times 10^{13}$	$\sim 3 \times 10^{13}$	$\sim 2 \times 10^{13}$
SSLS (Bahou *et al.*, 2007)	$\sim 3 \times 10^{13}$	$\sim 1 \times 10^{13}$	$\sim 8 \times 10^{12}$	$\sim 4 \times 10^{12}$
ALS (Barry *et al.*, 2002)		$\sim 7 \times 10^{12}$	$\sim 4 \times 10^{12}$	$\sim 2 \times 10^{12}$
SOLEIL (calculated) (Dumas *et al.*, 2006)	$\sim 1 \times 10^{14}$	$\sim 4 \times 10^{13}$	$\sim 1 \times 10^{13}$	$\sim 9 \times 10^{12}$

Figure 7
Spectral photon flux from MIRRORCLE-6FIR and a typical thermal source. The green and red lines are calculated and measured spectra, respectively. The measured photon flux was calibrated by a blackbody light source at 1500 K. The synchrotron radiation provides a much higher flux than that of the thermal source in the FIR/THz region.

is useful for broadband reflection and transmission spectroscopy from the THz to mid-IR regions.

4.4. Beam dynamics in MIRRORCLE-6FIR

Experimental study on the beam dynamics of MIRRORCLE-6FIR was performed by using FIR synchrotron radiation focused onto the beam trajectory by optical elements. The circulating beam current is about 1 A at 100 mA peak current and 400 Hz repetition injection. The capture ratio of the injected beam is very high, which is due to the resonance injection scheme (Takayama, 1987; Yamada, 1990). Almost 100% of the beam in a 200 ns time window is captured in this scheme.

Fig. 8 shows the PhSR output in the THz region using the Si bolometer at an injection rate of 15 Hz to show the lifetime of the beam. The vacuum pressure was 1.4×10^{-4} Pa. The time dependence signal is an exponentially decaying curve, which is usual for a SR source. For this large beam current one might expect a very short lifetime, but, according to the Touscheck lifetime calculation, around 1 min is the probable value. This long beam lifetime is due to the very large beam cross section

$(30 \times 3$ mm). The poor vacuum pressure caused this shortened beam lifetime.

Fig. 9 illustrates the radial distribution (along the horizontal axis) of the beam in a median plane as a function of the beam lifetime (vertical axis). Radiation distribution was scanned at the first focal point by changing the angle of the flat mirror, and the beam size at the source point was measured considering their respective distance from the concave mirror. The right-hand image is for the case when 100 W RF power is applied, and the left-hand one is for the case of no RF power. The radial beam size observed in this experiment is about ±15 mm before damping, but is reduced to about ±10 mm by applying an RF power of 100 W. When RF power is applied the beam always comes to the centre and beam damping appears. We can easily expect
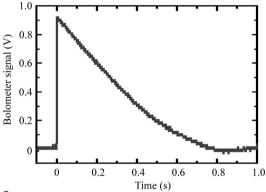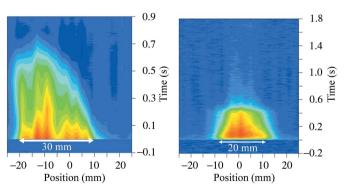

Figure 8
Beam lifetime of MIRRORCLE-6FIR measured using a cooled Si bolometer at 100 mA injection beam current and 15 Hz repetition rate. The observed 800 ms lifetime is quite large for such a low-energy storage ring, but the expected Touscheck lifetime is almost 1 min. The lifetime is limited by gas scattering owing to a poor vacuum pressure of 1.4×10^{-4} Pa.

Figure 9
Measured beam profiles in the radial direction (horizontal axis) as a function of the beam lifetime. This is observed by scanning the mirror angle at the first focal point. The right-hand image is for the case where 100 W RF power is applied, and the left-hand image is for the case of no RF power. Beam damping appears owing to the RF acceleration, and the beam size is reduced to ±10 mm.

that when RF is applied the photon intensity of MIRRORCLE-6FIR will increase by more than ten times. In the future we will fabricate the circular mirror and cavity in one piece.

5. Conclusion

We have presented details of the MIRRORCLE-6FIR beamline and characterized its performance. A circular optical system (PhSR) has been fabricated for MIRRORCLE-6FIR, and FIR measurements were performed with and without the PhSR. The PhSR designed has proved to work very well to boost the FIR intensity by an order of magnitude. Ray-tracing simulations, using computer code *ZEMAX*, were in good agreement with the experimental results, and helped optimize the optical system. We have also proven a highly coherent nature of the PhSR THz radiation owing to the high beam current and the PhSR optics. We have discussed that this coherence originates either by modulation of the beam owing to the interaction of the circulating photon beam and electron beam or by the very small radial beam size of the electron beam defined by the very small (0.2%) energy spread of the injector microtron.

The beamline is equipped with a Michelson-type FTIR for covering the spectral range 10–7800 cm^{-1}. The measured SR spectrum of MIRRORCLE-6FIR is significantly broader and much more intense than that of a typical blackbody light source. A large beam current and the special PhSR optics allow MIRRORCLE-6FIR, with its extremely small machine size, to provide comparable photon flux in the THz region with the large SR facilities. When RF power is applied together with the PhSR optics we expect more than one order higher flux than that of the current performance. We expect that all of these novel features will provide us with a new opportunity to perform various kinds of experiments useful for broadband reflection and far-infrared spectroscopy.

References

Bahou, M., Wen, L., Ding, X., Casse, B. D. F., Heussler, S. P., Gu, P., Diao, C., Moser, H. O., Sim, W. S., Gu, J. & Mathis, Y. L. (2007). *AIP Conf. Proc.* **879**, 603–606.

Barry, W. C. *et al.* (2002). *Proceedings of the 8th European Particle Accelerator Conference (EPAC 2002)*, Paris, France, pp. 656–657.

Byrd, J. M., Martin, M. C., McKinney, W. R., Munson, D. V., Nishimura, H., Robin, D. S., Sannibale, F., Schlueter, R. D., Thur, W. G., Jung, J. Y. & Wan, W. (2004). *Infrared Phys. Tech.* **45**, 325–330.

Chantry, W. (1971). *Submillimetre Spectroscopy*. New York: Academic Press.

Dumas, P., Polack, B., Lagarde, B., Chubar, O., Giorgetta, J. L. & Lefrancois, S. (2006). *Infrared Phys. Tech.* **49**, 152–160.

Duncan, W. D. & Williams, G. P. (1983). *Appl. Opt.* **22**, 2914–2923.

Ferguson, B. & Zhang, X. C. (2002). *Nat. Mater.* **1**, 26–33.

Fitch, A., Gates, P. N., Radcliffe, K., Dickson, F. N. & Bently, F. F. (1970). *Chemical Application of Far-Infrared Spectroscopy*. New York: Academic Press.

Hasegawa, D. & Yamada, H. (2007). *AIP Conf. Proc.* **902**, 19–22.

Hegelund, F., Wugt Larsen, R., Nelander, B., Christen, D. & Palmer, M. H. (2003). *J. Mol. Spectrosc.* **217**, 9–18.

Hirschmugl, C. J., Sagurton, M. & Williams, G. P. (1991). *Phys. Rev. A*, **44**, 1316–1320.

Ishi, K., Shibata, Y., Takahashi, T., Mishiro, H., Ohsaka, T. & Ikezawa, M. (1991). *Phys. Rev. A*, **43**, 5597–5604.

Keller, J. B. & Rubinow, S. I. (1960). *Ann. Phys.* **9**, 24–75.

Kimura, H. *et al.* (2001). *Nucl. Instrum. Methods Phys. Res. A*, **467–468**, 441–444.

Kimura, S., Nakamura, E., Nishi, T., Sakurai, Y., Hayashi, K., Yamazaki, J. & Katoh, M. (2006). *Infrared Phys. Tech.* **49**, 147–151.

Kleev, A. I., Manenkov, A. B. & Yamada, H. (1995). *Nucl. Instrum. Methods Phys. Res. A*, **358**, 362–364.

Lobo, R. P. S. M., LaVeigne, J., Reitze, D. H., Tanner, D. B. & Carr, G. L. (1999). *Rev. Sci. Instrum.* **70**, 2899.

Martin, M. C. & McKinney, W. R. (2001). *Ferroelectrics*, **249**, 1–10.

Michel, F. C. (1982). *Phys. Rev. Lett.* **48**, 580–583.

Mima, K., Shimoda, K. & Yamada, H. (1991). *IEEE J. Quant. Electron.* **27**, 2572–2577.

Miura, N., Moon, A., Yamada, H. & Kitagawa, T. (2007). *AIP Conf. Proc.* **902**, 73–76.

Moon, A., Miura, N., Yamada, H. & Monirul Haque, M. (2007). *AIP Conf. Proc.* **902**, 23–25.

Muller, R., Hoehl, A., Klein, R., Ulm, G., Schade, U., Holldack, K. & Stefeld, G. W. (2006). *Infrared Phys. Tech.* **49**, 161–166.

Schade, U., Roseler, A., Korte, E. H., Bartl, F., Hofmann, K. P., Noll, T. & Peatman, W. B. (2002). *Rev. Sci. Instrum.* **73**, 1568–1570.

Surman, M., Flaherty, J., Burrows, I., Nunney, T. S., Roberts, A. J., Carew, A. J., Middleman, K., Raval, R., Wilson, N. E. & Russell, A. E. (1999). *Proc. Soc. Photo-Opt. Instrum. Eng.* **3775**, 156–166.

Takayama, T. (1987). *Nucl. Instrum. Methods Phys. Res. B*, **24/25**, 420–424.

Weinstein, L. A. (1969). *Open Resonators and Open Waveguides*. Boulder: Golem.

Williams, G. P. (2002). *Rev. Sci. Instrum.* **73**, 1461–1463.

Wingham, D. J. (1987). *Phys. Rev. D*, **35**, 2584–2594.

Yamada, H. (1989). *Jpn. J. Appl. Phys.* **28**, L1665–L1668.

Yamada, H. (1990). *J. Vac. Sci. Technol. B*, **8**, 1628–1631.

Yamada, H. (1991). *Nucl. Instrum. Methods Phys. Res. A*, **304**, 700–702.

Yamada, H. (1997). *Adv. Colloid Interface Sci.* **71/72**, 371–392.

Yamada, H. (1998). *J. Synchrotron Rad.* **5**, 1326–1331.

Yamada, H. (2003). *Nucl. Instrum. Methods Phys. Res. B*, **199**, 509–516.

Yamada, H. (2004). *AIP Conf. Proc.* **716**, 12–17.